Pergamon

PII: S0301-9322(96)00023-7

Int. J. Multiphase Flow Vol. 22, No. 6, pp. 1035–1053, 1996

0301-9322/96 $15.00 + 0.00

GAS–LIQUID FLOW PATTERNS IN MICROGRAVITY: EFFECTS OF TUBE DIAMETER, LIQUID VISCOSITY AND SURFACE TENSION

W. S. BOUSMAN[1], J. B. McQUILLEN[2] and L. C. WITTE[3]

[1]Department of Chemical Engineering, University of Houston, Houston, TX 77204-4792, U.S.A.
[2]NASA Lewis Research Center, Cleveland, OH 44135, U.S.A.
[3]Department of Mechanical Engineering, University of Houston, Houston, TX 77204-4792, U.S.A.

(Received 27 September 1995; in revised form 28 April 1996)

Abstract—Two-phase gas–liquid flow experiments have been developed for use on NASA microgravity aircraft to allow for high speed measurement of void fraction, liquid film thickness and pressure drop as well as high-speed photography of the flow features. Numerous experiments were conducted in order to determine the effect of liquid and gas superficial velocities, tube diameter, liquid viscosity and surface tension on the occurrence of flow patterns in microgravity. The transition from bubble to slug flow was found to be affected by tube diameter for air–water and by changes in liquid viscosity and surface tension. The transition from slug to annular flow was not significantly affected by changes in tube diameter, liquid viscosity or surface tension. Void fraction based transition models were developed to predict microgravity flow patterns. Weber number based transition models were also evaluated. Copyright © 1996 Elsevier Science Ltd.

Key Words: microgravity, two-phase flow, flow patterns

1. INTRODUCTION

Two-phase gas–liquid flows are expected to occur in a number of future space operations including the design and operation of spacecraft environmental systems, storage and transfer of cryogenic fluids and safety and performance issues related to space nuclear power systems (Swanson *et al.* 1989). With the lack of buoyancy in the microgravity environment, gas–liquid flows have been shown to behave differently from those on earth (Dukler *et al.* 1988). Thus gas–liquid flow models and systems developed in earth gravity may not function as expected in the microgravity environment.

Gas–liquid flows distribute themselves into one of several distinct flow patterns depending primarily on the flow rates of gas and liquid, the physical properties of the phases and the magnitude and orientation of gravity. The flow patterns observed in microgravity during the course of this study are represented graphically in figure 1. Because of the differences between flow patterns, modeling of gas–liquid flow characteristics has generally been more successful when applied to a single flow pattern rather than to the entire set of flow patterns. Therefore, knowledge of the flow pattern that could occur under a given set of conditions generally leads to better predictions of gas–liquid flow behavior.

The occurrence of the various flow patterns as a function of gas and liquid flow rates is well established for gas–liquid flows in earth gravity for horizontal, vertical and inclined flows (Baker 1954; Taitel & Dukler 1976; Barnea 1986). Comparison of these works shows that the magnitude and orientation of the gravity vector with respect to the flow direction has a significant effect on the resulting flow patterns. Therefore, establishing flow pattern maps for microgravity gas–liquid flows is a necessary first step in developing a better understanding of these flows.

2. PREVIOUS WORK

The first microgravity flow pattern map to span a large area of the liquid and gas superficial velocity parameter space was presented by Dukler *et al.* (1988) for air–water in a 12.7 mm ID tube. This study was conducted during the early development phase of the NASA Learjet flow loop and

test sections used in the present study. The flow map contains only 21 data points but begins to resolve the occurrence of the flow patterns across the gas–liquid superficial velocity parameter space. An expanded version of the Dukler *et al.* flow pattern map for air–water, containing an additional 14 data points, was presented by Janicot (1988). These additional data further improve the resolution of the flow patterns. These two studies provided the foundation for the present study.

An extensive study of the bubble and slug flow regimes in microgravity for air–water in a 40 mm ID tube was presented by Colin (1990) and Colin *et al.* (1991). The flow pattern map clearly resolves the bubble and slug flow regions of the gas–liquid parameter space.

Huckerby & Rezkallah (1992) presented a microgravity air–water flow pattern mapping study in a 9.525 mm ID tube. As shown, this study spans essentially the same gas–liquid velocity parameter space as that of Janicot (1988). With minor exceptions, the 9.525 mm ID results of Huckerby & Rezkallah are in fair agreement with the 12.7 mm ID results of Janicot (1988). This study was followed by a more comprehensive air–water microgravity flow pattern map presented in Zhao & Rezkallah (1993). These results are in good agreement with those of Janicot (1988) except for the bubble–slug transition region.

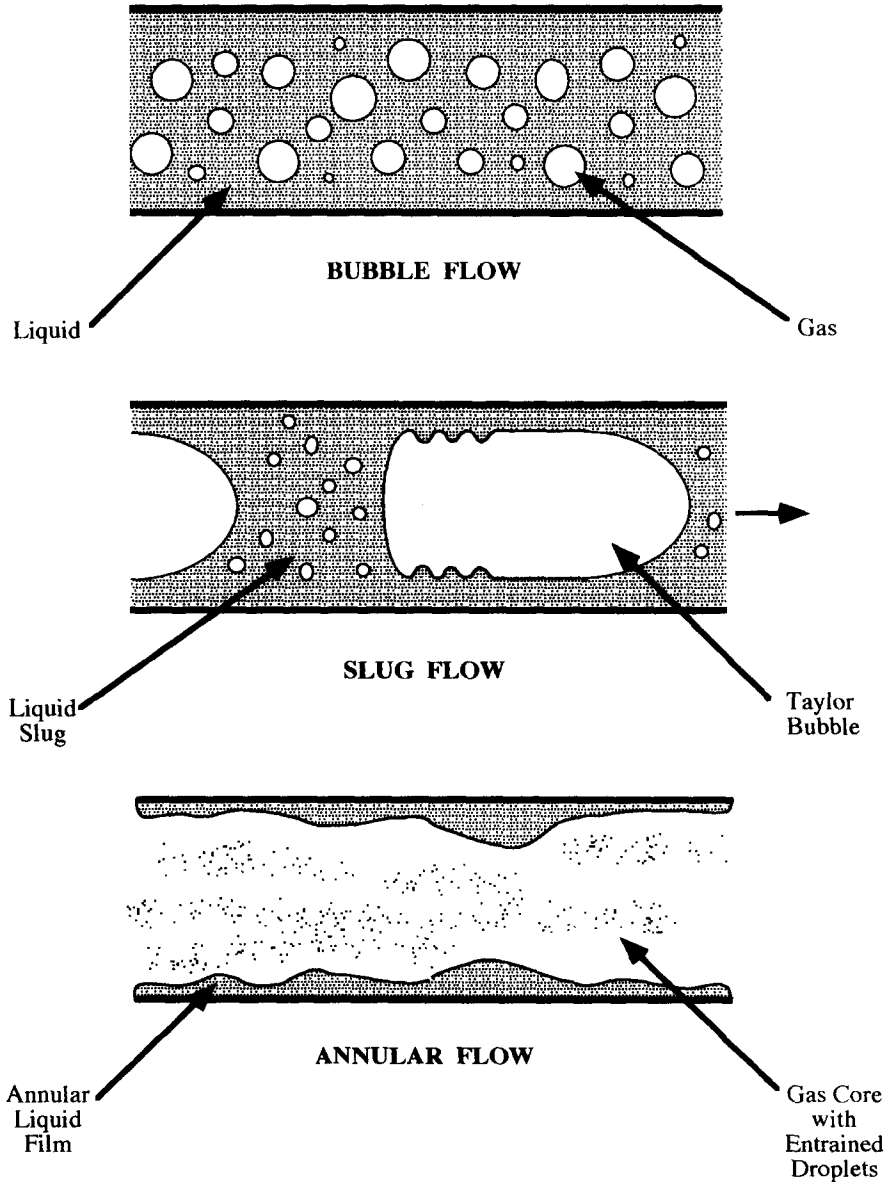

Figure 1. Two-phase flow patterns observed in microgravity.

Another recent flow pattern mapping effort was that of Reinarts (1993) for R12 in 4.7 and 10.5 mm ID tubes. Only the annular flow region of the gas–liquid parameter space was mapped for the 4.7 mm ID tube. The flow pattern map for R12 in a 10.5 mm ID tube is much more complete and spans a large parameter space. The locations of the flow pattern boundaries are clearly different from those of the previous air–water studies with the annular flow regime occurring at much lower void fractions for R12 than for air–water. The gas to liquid density ratio is much greater for R12 than for air–water, suggesting that the densities of the phases are important factors in flow pattern determination.

3. EXPERIMENTAL APPARATUS

For this study, the microgravity environment was attained by using both the Learjet Model 25 aircraft based at the NASA Lewis Research Center and the KC-135 aircraft based at the NASA Johnson Space Center. By following a parabolic flight path, these aircraft can produce periods of microgravity lasting 15–25 s (Lekan 1989). To monitor the quality of the microgravity environment produced on the aircraft, accelerations were measured in all three axes on the experimental apparatus, accurate to 0.001 g. The experiment was considered to be in microgravity when the acceleration was less than $\pm 0.02\,g$ in all three dimensions. The data reported in this study satisfied this condition. The duration of the experiments was typically 7–20 s.

Flow loops for the Learjet and KC-135 aircraft, shown schematically in figures 2 and 3, respectively, were constructed to provide metered quantities of gas and liquid to the test sections used in these studies (Bousman 1995). The gas flow rate was controlled with a critically-choked orifice in order to make the flow rate independent of downstream pressure changes (McQuillen & Neumann 1995). The uncertainty in the gas superficial velocity measurement was estimated to be less than 8% over the range investigated in these studies. A steady flow rate of liquid was provided using a pressure-loaded piston in the liquid feed tank. The uncertainty in the liquid superficial velocity measurement was estimated to be less than 10% over the range investigated in this study. The gas and liquid were combined in an annular mixer with the gas entering in the center and the liquid in the annulus to produce a gas core surrounded by a liquid film. In the Learjet flow loop, the two-phase mixture passed through a 1.1 m long, 11.2 mm ID flow development section prior to entering the test section. The test section used on the KC-135 flow loop contained 25.4 mm ID flow development sections within it and provided 2 m of flow development prior to the portion of the test section containing the photography window and probes used in this study. At the exit of the test section, the mixture was separated over screens by surface tension and the liquid was recovered for reuse while air was vented into the cabin. Control of flow loop functions as well as data acquisition and storage is accomplished with a dedicated computer in the flow loop rig.

A 12.7 mm ID test section, shown in figure 4, for use on the Learjet consisted of a smooth acrylic tube to which several probes were attached. A 25.4 mm ID test section of similar construction, shown in figure 5, was constructed for use on the KC-135 aircraft. The liquid film thickness and void fraction conductivity probes, shown in figure 6, were based on the parallel wire conductance method originally described by Brown *et al.* (1978) and described in detail in Bousman (1995). As shown, the conductivity probes consist of a pair of closely spaced parallel wires stretched tightly across the tube cross section. High-speed conductivity electronics were used to produce a high frequency alternating voltage (10 kHz) across the wires, allowing measurement of the conductivity between the wires (Lacy 1992). By using aqueous fluids, which were made conductive by adding a small amount of sodium chloride, the conductivity measurement system provides a voltage output which is linearly proportional to the liquid film thickness or void fraction, depending on the calibration. The film thickness and void fraction data were acquired at 1000 Hz, far below the 1850 Hz measured dynamic response for the conductance system. Based on calibration measurement errors and electronic discretization errors, the uncertainty in the void fraction measurement was estimated to be ± 0.01 while the uncertainty in the film thickness measurement was estimated to be ± 0.02 mm. The water-filled viewing box allowed for high-speed photography of the flow with minimal refractive distortion. Photographic images were acquired at 400 frames per second.

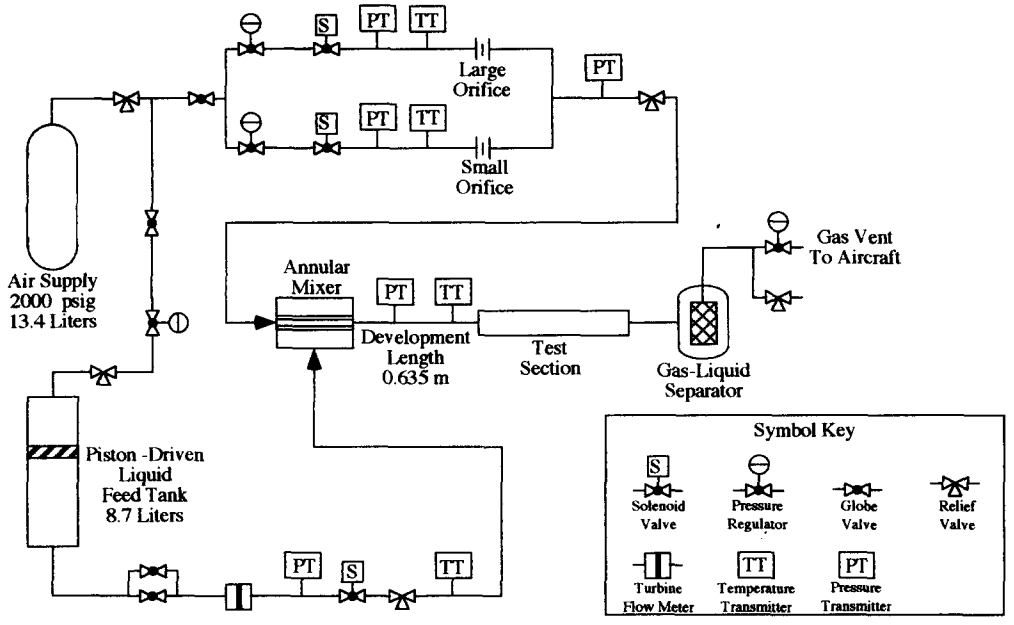

Figure 2. Flow loop used on the NASA Learjet for the 12.7 mm ID test sections.

4. FLOW PATTERN IDENTIFICATION

While the idealized microgravity flow patterns shown in figure 1 are easily distinguished from one another, identifying the flow patterns in real two-phase flows can be difficult, especially for high superficial gas velocities where small flow features can travel in excess of 5 m/s. In addition, the transition from one flow pattern to another appears to be a zone of continuous change from one predominate pattern to the other rather than a discrete boundary. As a result, flow pattern identification remains partially subjective and this is responsible for some of the discrepancy in flow pattern transitions reported in the literature. Previous microgravity flow pattern studies in the

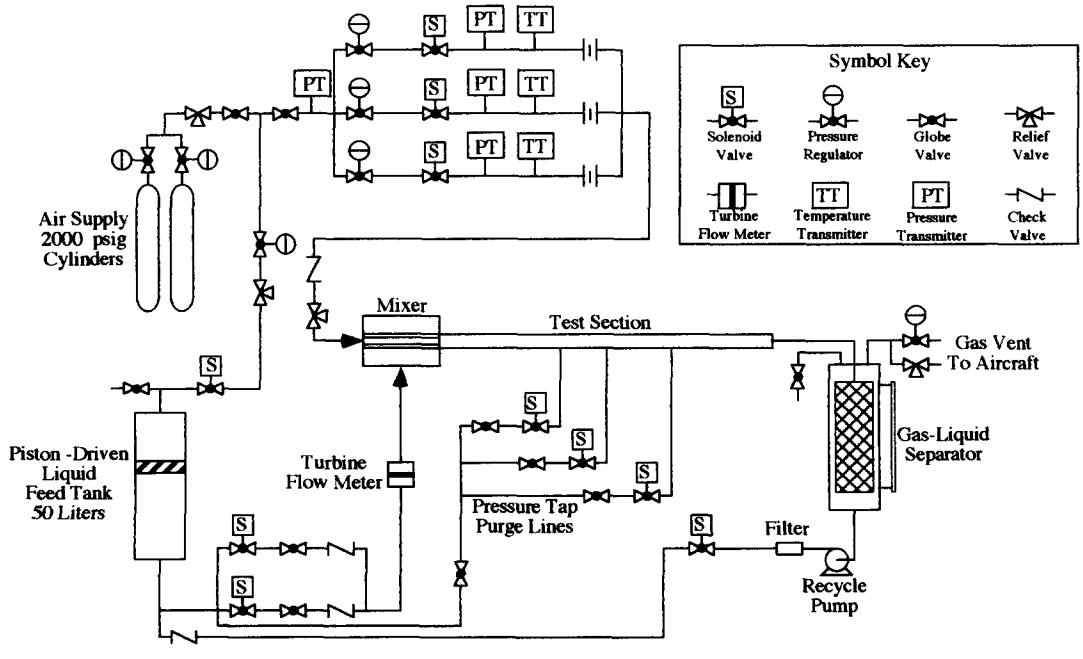

Figure 3. Flow loop used on the NASA KC-135 Aircraft for the 25.4 mm ID test section.

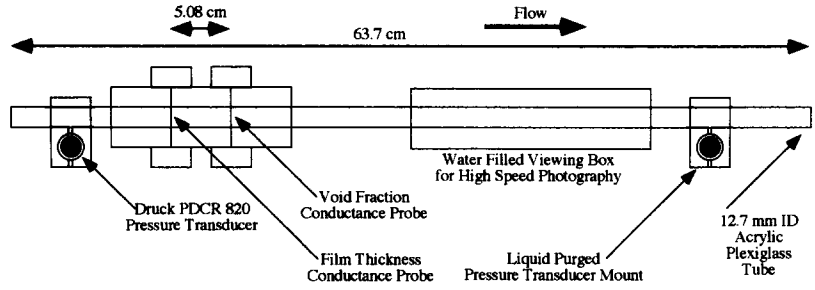

Figure 4. 12.7 mm ID test section.

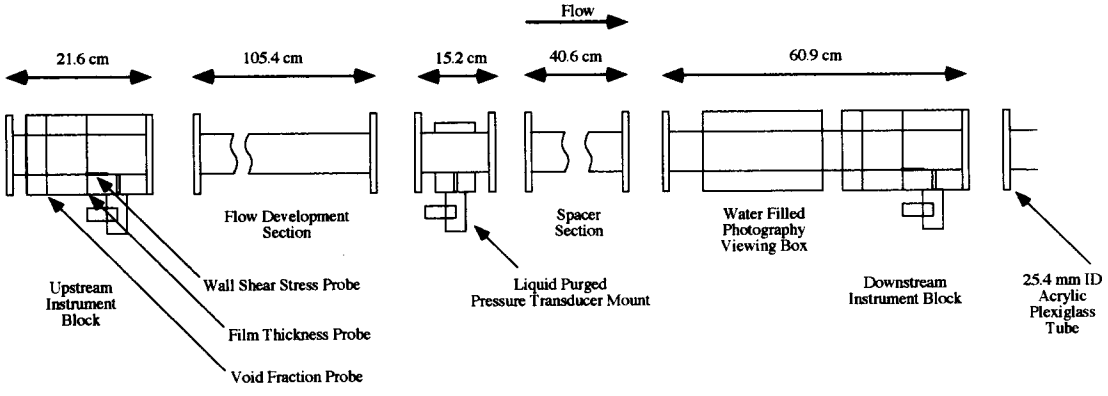

Figure 5. 25.4 mm ID test section.

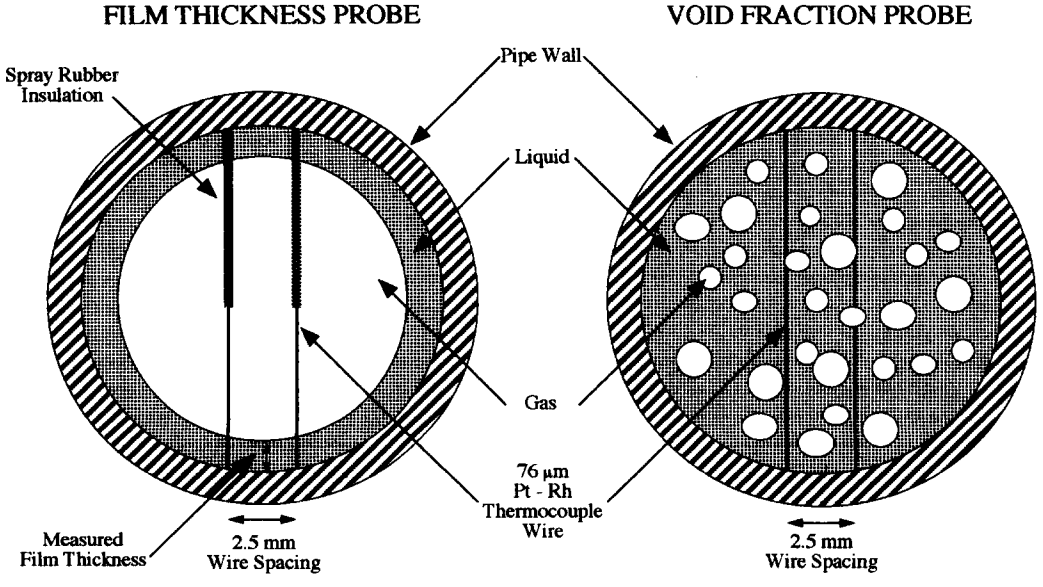

Figure 6. Parallel wire conductance probes for film thickness and void fraction measurement.

literature have relied primarily on photography to identify flow patterns. In the current study, it was found that a combination of photography and electronic liquid film thickness and void fraction measurements were needed to better identify flow patterns.

Typical photographs of bubble, slug and annular flows as well as bubble–slug and slug–annular transition states are shown in figures 7–11. As shown in figure 7, the flow pattern was identified as bubble when the gas phase existed as discrete, nearly-spherical bubbles. This flow pattern was usually identified photographically, although this flow pattern also possessed a distinctive void fraction time trace. Slug flows were differentiated from bubble flows by the presence of Taylor bubbles which were longer than the tube diameter, as shown in figure 9. This flow pattern was identified using a combination of photography and electronic film thickness traces. A typical microgravity slug flow film thickness time series trace, shown in figure 12, clearly shows the presence of Taylor bubbles and liquid slugs. A transitional flow pattern identified as bubble–slug was also observed in a few cases. As shown in figure 8, this transitional state exhibits characteristics of each

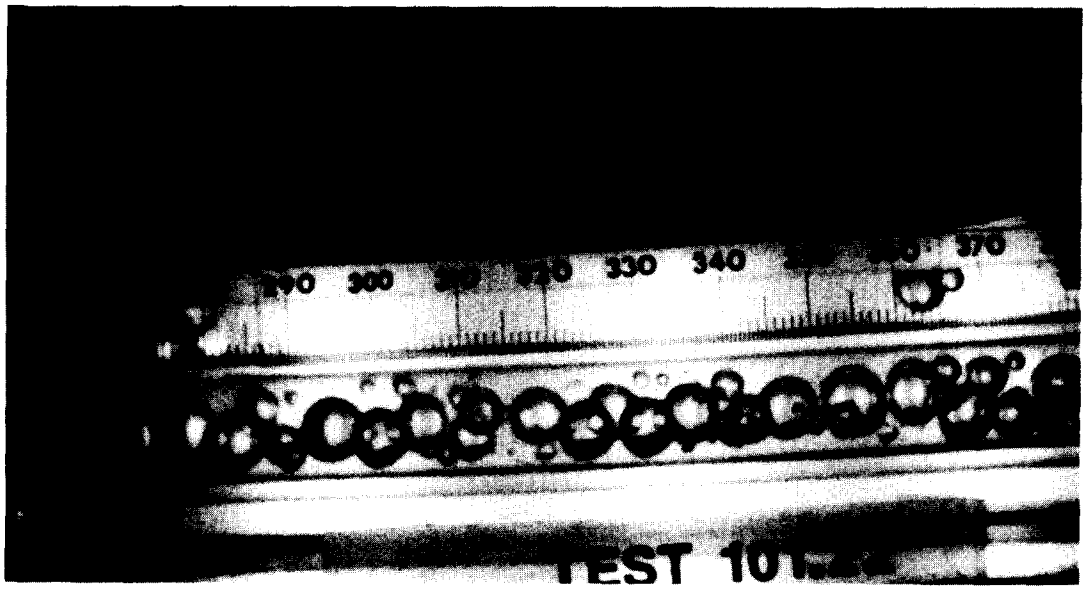

Figure 7. Photograph of microgravity air–water/Zonyl FSP bubble flow in a 12.7 mm ID tube.

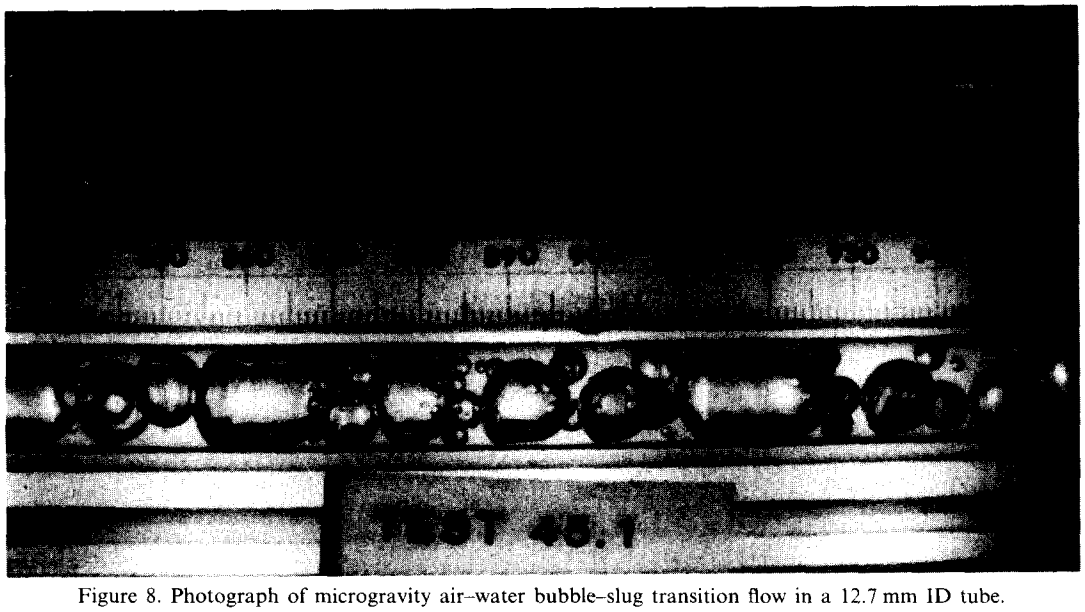

Figure 8. Photograph of microgravity air–water bubble–slug transition flow in a 12.7 mm ID tube.

adjacent flow pattern intermittently. This transition state was also identified primarily by photography.

As shown in figure 11, the features of annular flows were difficult to resolve photographically and these flow patterns were usually identified using electronic film thickness time traces. A typical microgravity annular flow film thickness time series, shown in figure 13, shows the presence of a wavy film with a continuous gas core. Slug flows were differentiated from annular flows by the presence of liquid slugs which bridged the tube. These slugs were often very short and could only be observed using the electronic film thickness measurements. A transitional state between slug and annular flow was also observed, as shown in figure 10. This flow pattern was characterized by large amplitude waves which momentarily bridged the tube to form liquid slugs and then collapsed. These tube bridging events were often difficult to identify from electronic film thickness measurement because the short-lived events usually did not occur at the same location as the film thickness wires. It was observed however that when the amplitude of the waves exceeded 70% of

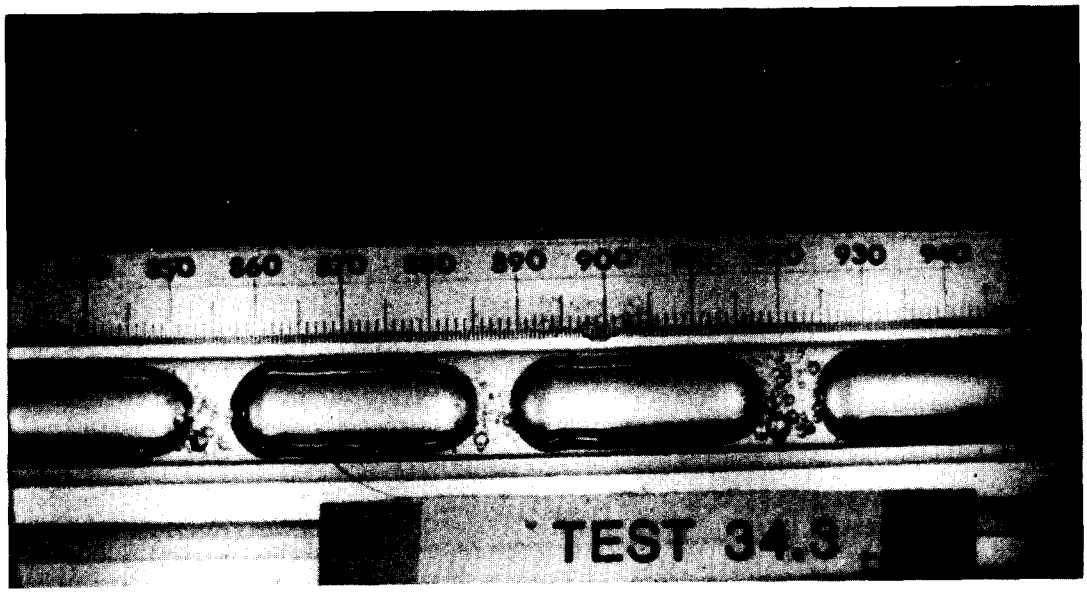

Figure 9. Photograph of microgravity air–water slug flow in a 12.7 mm ID tube.

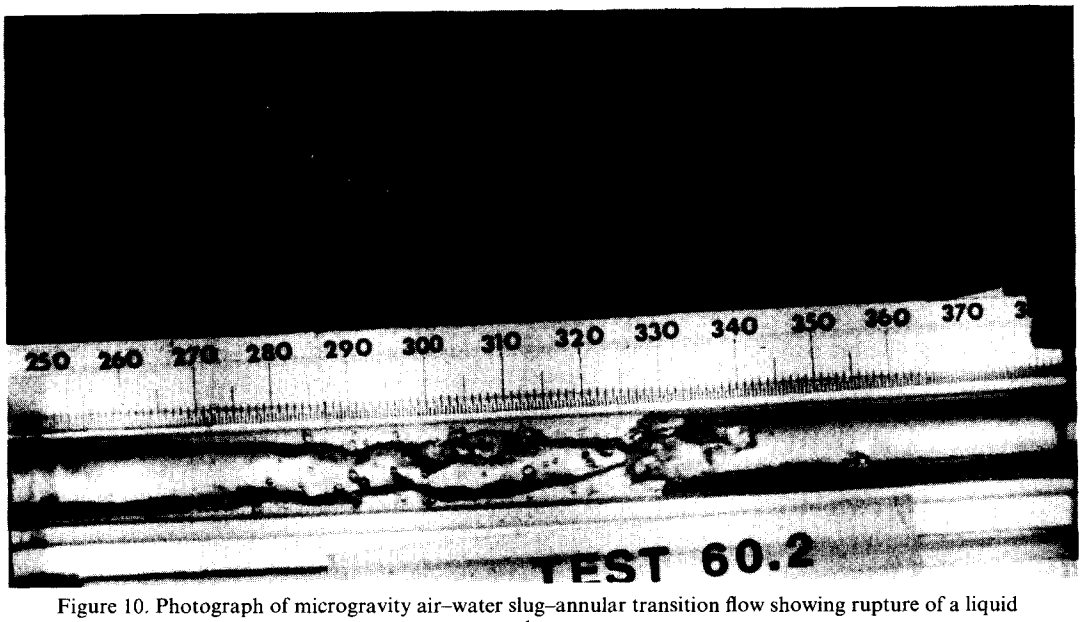

Figure 10. Photograph of microgravity air–water slug–annular transition flow showing rupture of a liquid slug.

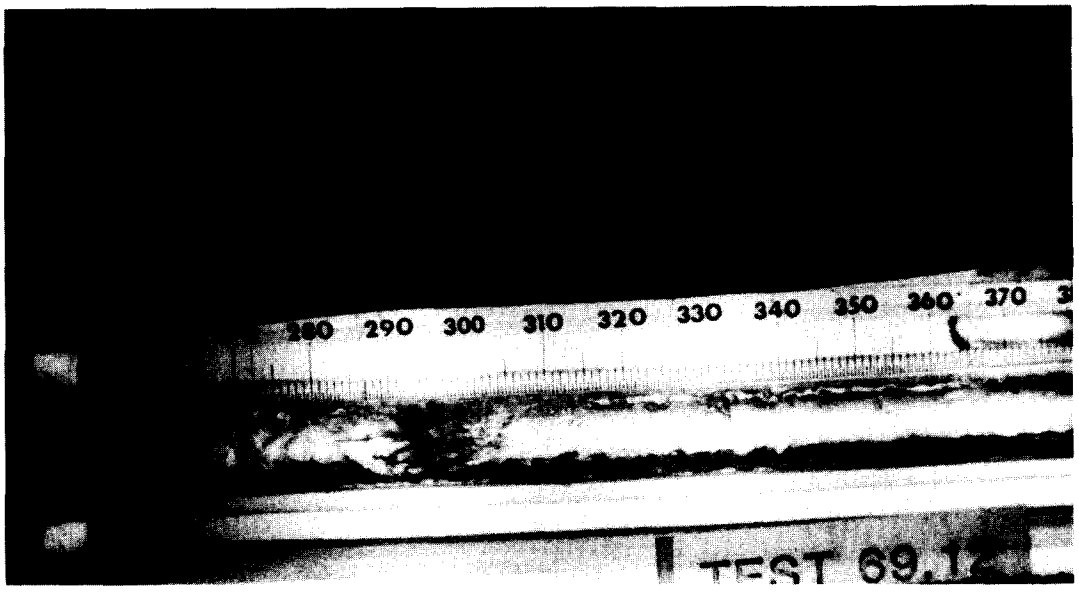

Figure 11. Photograph of microgravity air–water annular flow in a 12.7 mm ID tube.

the tube diameter, tube bridging events could usually be found in the photographs. An example of a film thickness trace for this transitional state is shown in figure 14.

5. FLOW PATTERN MAPPING RESULTS

The experimental apparatus was used over the course of many aircraft flights to establish flow pattern maps in microgravity as a function of liquid viscosity, surface tension and tube diameter, which were thought to be three of the key parameters affecting the flow pattern maps. To test the effects of liquid viscosity and surface tension on the occurrence of the flow patterns, three liquids were tested (all at $21 \pm 2°C$) water ($\mu = 1$ cP, $\sigma = 72$ dynes/cm), 50–50 wt% water/glycerin ($\mu = 6$ cP, $\sigma = 63$ dynes/cm) and water/Zonyl FSP ($\mu = 1$ cP, $\sigma = 21$ dynes/cm). Zonyl FSP (DuPont) is a powerful surfactant which, when used in low concentrations (0.5 wt% in these studies), lowers the surface tension to 21 dynes/cm without significantly affecting the other physical properties of the liquid. The Reinarts (1993) study with Freon indicates that the density of the gas phase relative to the liquid phase has a significant effect on the flow pattern maps. Large changes in gas density as compared with the air used in this study were not investigated however because the use of a high pressure flow loop or dense gases such as Freon on board the NASA aircraft would add considerable complexity to the design and operation of the apparatus and prevent some of the measurements taken in this study from being made. To determine the effect of tube diameter, flow pattern maps for all three liquids were established for 12.7 mm and 25.4 mm ID tubes.

The flow pattern maps for both tube diameters and all three fluid systems are shown in figures 15–20. As shown by comparing figure 15 to figure 18, the change in tube diameter leads to a shift in the bubble–slug transition to lower values of U_{GS}, and thus void fraction, for the air–water system. For the air–water/glycerin and air–water/Zonyl FSP systems, the change in tube diameter produced no significant change in the location of the bubble–slug transition. For all three fluid systems, the change in tube diameter had little effect on the location of the slug–annular transition.

Comparison of the air–water and air–water/glycerin flow pattern maps shows that a six-fold increase in the liquid viscosity produced no significant change in the location of either flow pattern transition for the 12.7 mm ID tube. The same increase in liquid viscosity in the 25.4 mm ID tube produces a shift in the bubble–slug transition to higher void fractions but again has no effect on the location of the slug–annular transition. Comparison of the air–water and air–water/Zonyl FSP maps shows that reducing the surface tension results in a shift in the bubble–slug transition to higher void fraction suggesting that surface tension plays a role in the bubble to slug transition mechanism. The change in surface tension had no significant effect on the slug–annular transition.

With the flow pattern mapping results of this study established, it is useful to compare these maps to those in previous works. The air–water flow pattern map for the 12.7 mm ID tube shown in figure 15 is in good agreement with the maps presented by Dukler *et al.* (1988) and Janicot (1988). This result is expected since all three studies used similar apparatus and techniques.

The location of the transition between bubble and slug flow on the air–water microgravity flow pattern map of Colin (1990) for a 40 mm ID tube compares well to the 25.4 mm ID air–water flow pattern map, figure 18, in the present study.

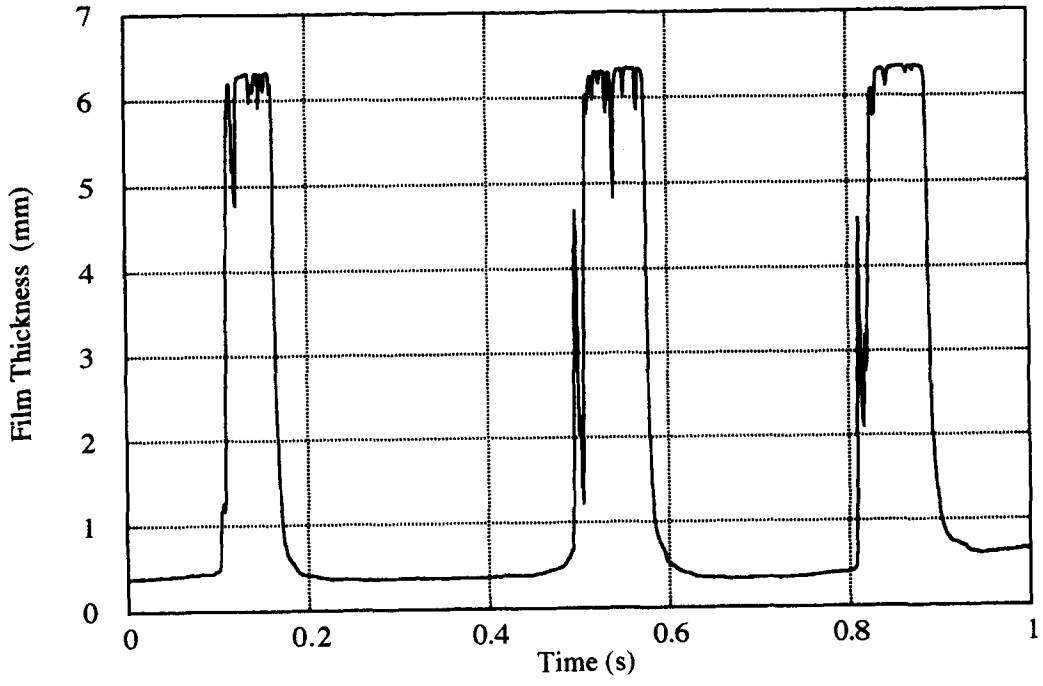

Figure 12. Typical film thickness time series trace of slug flow in microgravity.

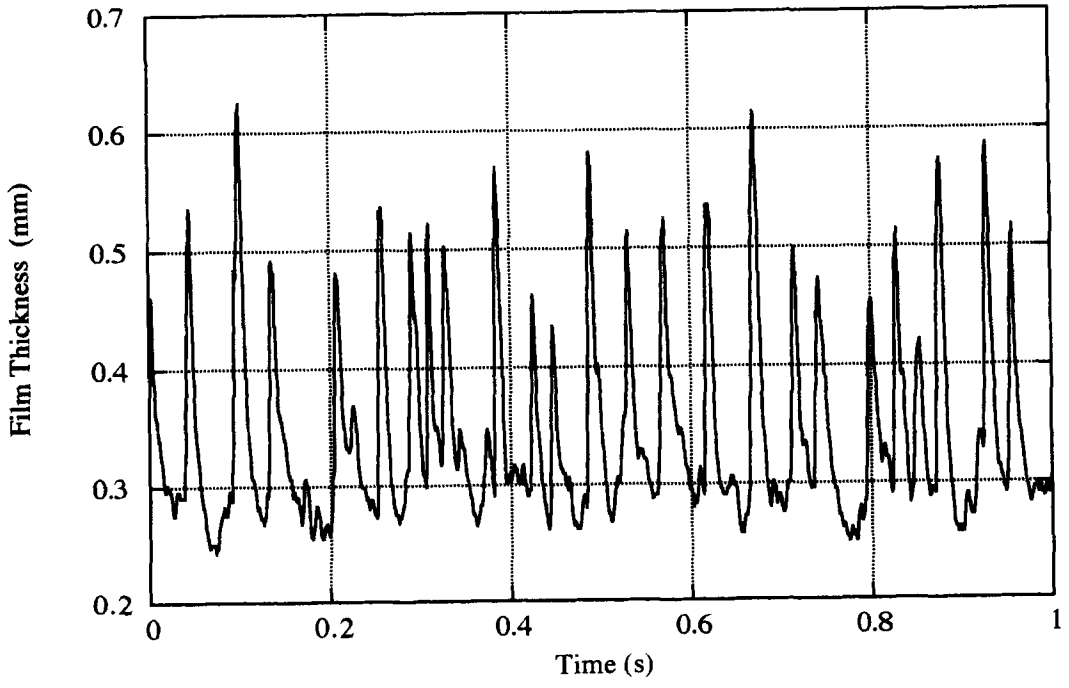

Figure 13. Typical film thickness time series trace of annular flow in microgravity.

The results of Huckerby & Rezkallah (1992) for air–water in a 9.525 mm ID tube show fair agreement with the 12.7 mm ID tube air–water results, figure 15, in the present study. The Huckerby & Rezkallah map shows the bubble–slug transition to be nearly independent of the gas superficial velocity, U_{GS}, which is contrary to the findings of the present study. The slug and annular regions of both flow maps are similar.

The Zhao & Rezkallah (1993) study for air–water in a 9.525 mm ID tube shows the bubble–slug transition region to be significantly different than that of the Huckerby & Rezkallah (1992) flow pattern map or the present 12.7 mm ID tube, air–water map in figure 15. The cause of this discrepancy is unexplained but could be due to a difference in the identification criteria. The location of the slug–annular transition reported in Zhao & Rezkallah (1993) is in good agreement with the results in figure 15.

6. VOID FRACTION FLOW PATTERN TRANSITION MODELS

In addition to establishing flow pattern maps, it is useful to develop models which predict the location of the transitions on the maps. For microgravity gas–liquid flow pattern transitions, two approaches have been suggested: a void fraction criteria from Dukler *et al.* (1988) and a Weber number criteria from Zhao & Rezkallah (1993). Both were examined in relation to the current study.

The void fraction based model for the bubble–slug transition was developed by examining the high speed movie images of the experiments near the transition. These films suggested that the transition from bubble to slug flow occurred when spherical bubbles became so densely packed that they touched and coalesced. This implies that the transition occurs at a constant void fraction. The maximum packing density of rigid spheres in a cylindrical tube is 52%, which imposes an upper limit on the transition void fraction. However, oscillations in the shape and position of the bubbles due to turbulence give the bubbles a larger effective diameter and allow for coalescence at lower void fractions.

The mean void fraction values measured for bubble–slug transition flows in a 12.7 mm ID tube were found to lie in a distinct range between those of the bubble and slug flow experiments. The

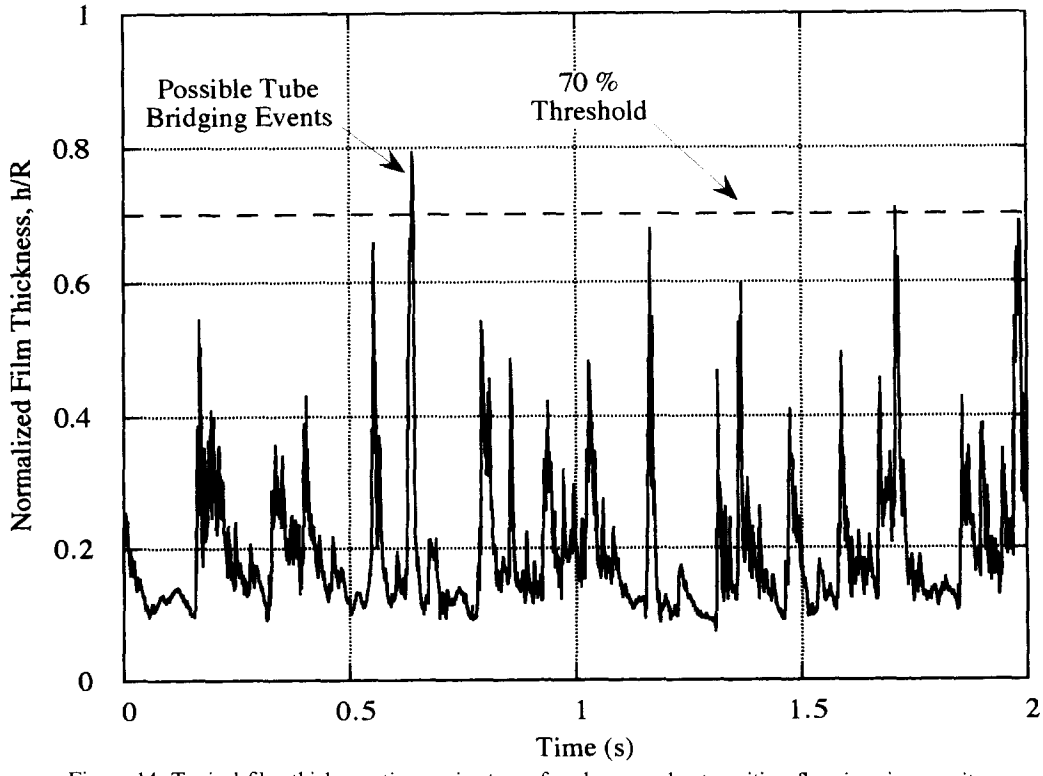

Figure 14. Typical film thickness time series trace for slug–annular transition flow in microgravity.

center point of this range was used as the characteristic void fraction for the transition. Since adequate void fraction measurements were not available for the experiments conducted in the 25.4 mm ID tube, the void fraction of each transition run was estimated using the drift–flux model (Zuber & Findlay 1965) with a distribution coefficient determined from the 12.7 mm ID tube experiments (Bousman 1995). From these estimated void fractions, the transition void fraction was determined for each flow pattern map. The transition void fraction value for each tube diameter and fluid system is shown in table 1.

The drift–flux model with a drift velocity of zero (due to the lack of buoyancy between phases in microgravity) leads to

$$U_{LS} = \frac{(1 - C_0\langle\varepsilon\rangle)}{C_0\langle\varepsilon\rangle} U_{GS}, \qquad [1]$$

where C_0 is the distribution coefficient defined by Zuber & Findlay (1965), $\langle\varepsilon\rangle$ is the cross-sectional average void fraction and U_{LS} and U_{GS} are the liquid and gas superficial velocities respectively. The distribution coefficient C_0 was determined to be 1.21 for microgravity gas–liquid flows using experimental void fraction measurements (Bousman 1995). Using this in conjunction with the transition void fraction values in table 1 yields lines of constant void fraction on the flow pattern maps which represent the predicted bubble–slug transition.

The bubble–slug transition predicted from the void fraction matching criteria is superimposed on the flow pattern maps in figures 15–20. As shown, these lines of constant void fraction separate the bubble and slug regions of the flow map, which is expected since these models were derived from the data. With the exception of the air–water flow pattern map for the 25.4 mm ID tube, the bubble–slug transition occurs at a void fraction of about 40%.

The large decrease in transition void fraction for the air–water system in the larger diameter tube is also present in the flow pattern map presented by Colin (1990) for air–water in a 40 mm ID tube. To better understand this result, the movie films of the experiments near the transition were examined for both the small and large tubes. In the 25.4 mm ID tube, the gas–liquid bubble interfaces were in a continuous state of fluctuation while those in the 12.7 mm ID tube under the same flow conditions were more stable. These oscillations in the larger tube, which can be attributed

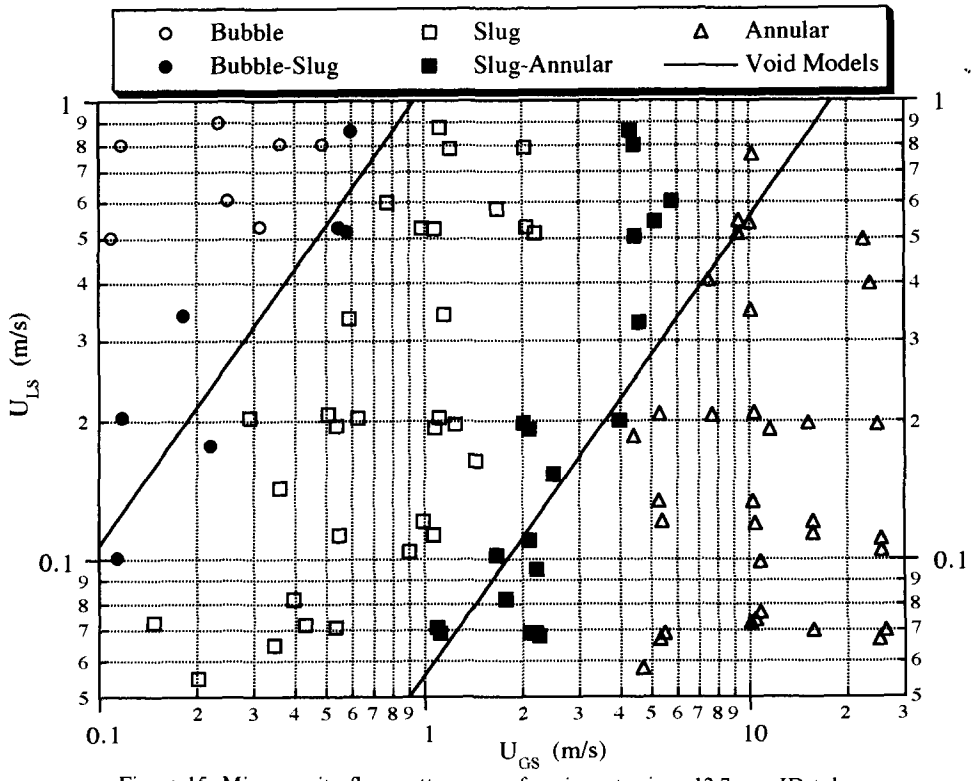

Figure 15. Microgravity flow pattern map for air–water in a 12.7 mm ID tube.

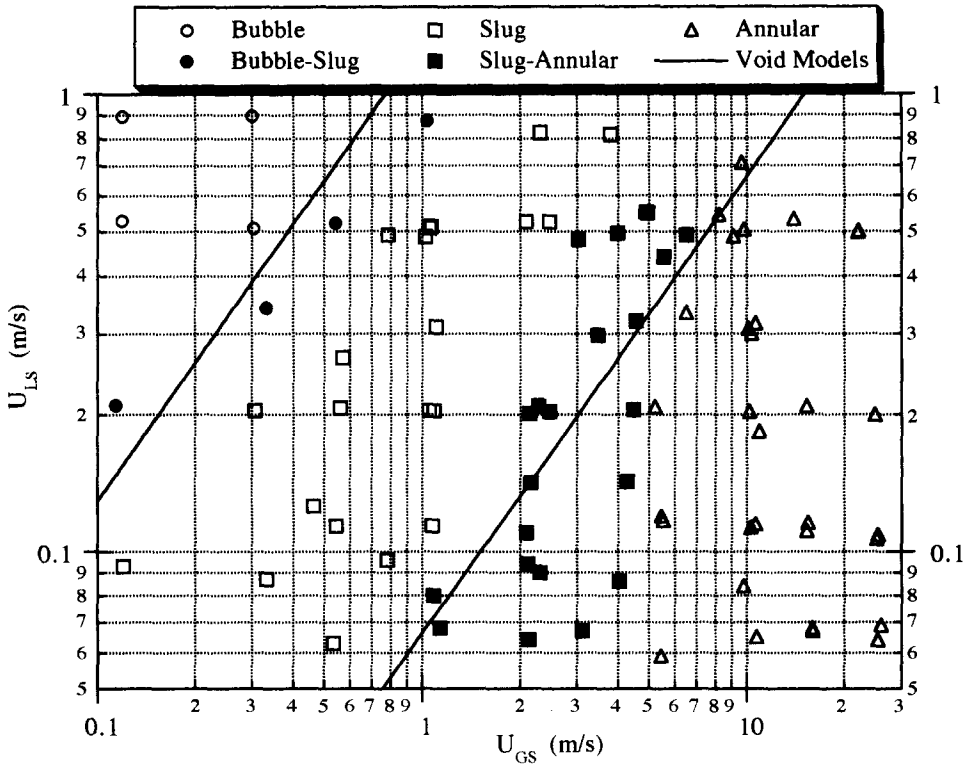

Figure 16. Microgravity flow pattern map for air–water/glycerin in a 12.7 mm ID tube.

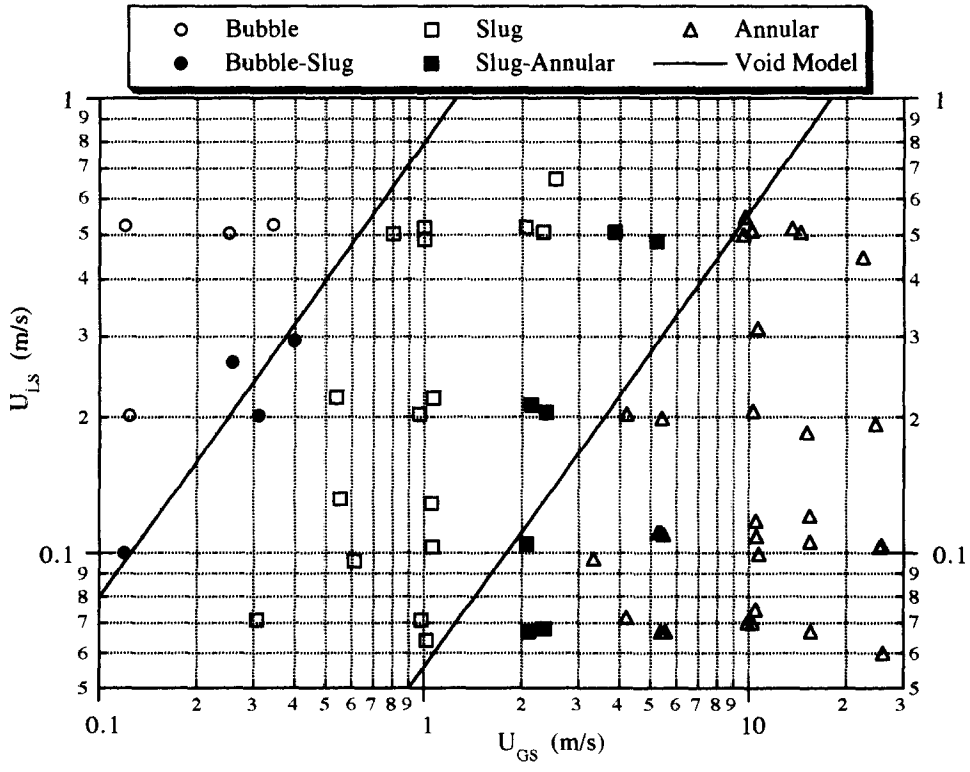

Figure 17. Microgravity flow pattern map for air–water/Zonyl FSP in a 12.7 mm ID tube.

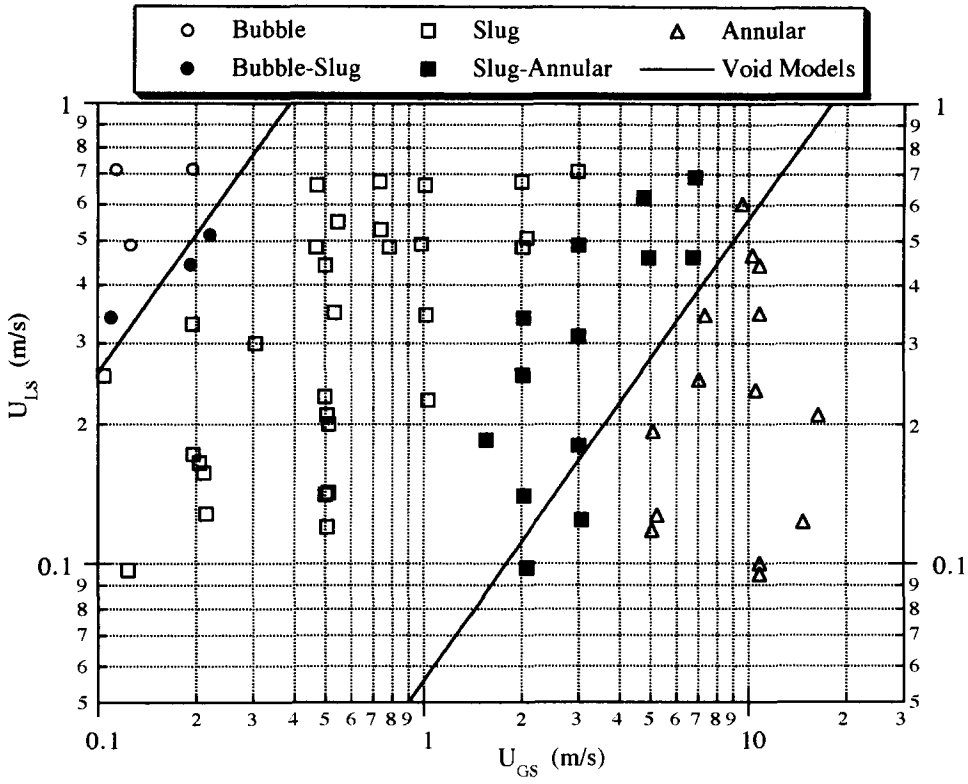

Figure 18. Microgravity flow pattern map for air–water in a 25.4 mm ID tube.

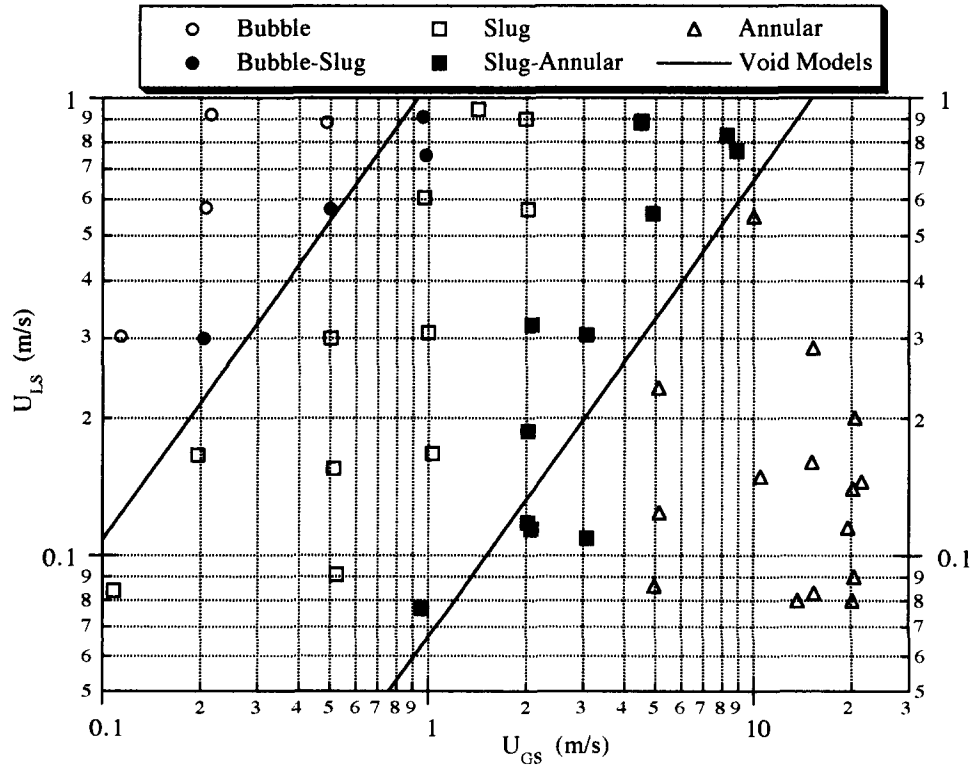

Figure 19. Microgravity flow pattern map for air–water/glycerin in a 25.4 mm ID tube.

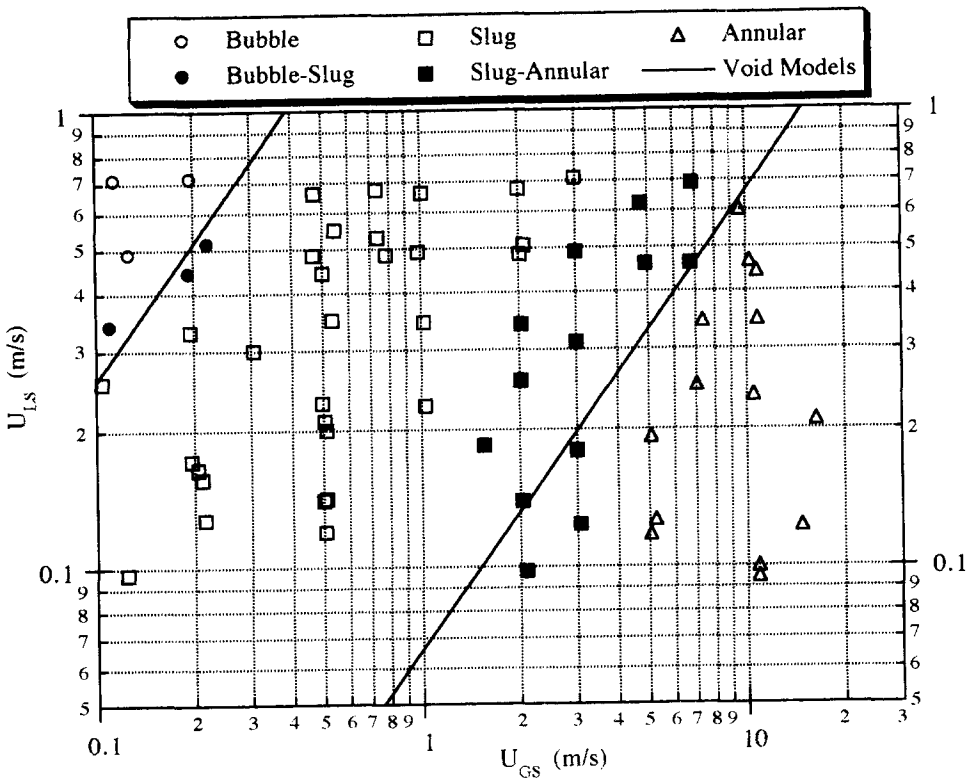

Figure 20. Flow pattern map for air–water/Zonyl FSP in a 25.4 mm ID tube.

to turbulence, give the bubbles a larger effective diameter thus increasing the probability of contacting nearby bubbles. The result is a transition to slug flow at a lower void fraction. This effect was not observed in the air–water/glycerin experiments in the large tube due to a reduction in turbulence and consequently the reduction in the bubble–slug transition void fraction was not observed in the air–water/glycerin system. The reduced surface tension in the air–water/Zonyl experiments should reduce the probability of coalescence when bubbles contact each other and this may explain why the decrease in transition void fraction was not observed for this system in the larger tube even when the strong bubble oscillations were present.

A void fraction transition model for the slug–annular transition was developed by Bousman (1995) using force balances to determine a void fraction relationship for annular flow. By equating this with the slug flow void fraction expression developed from the drift–flux model, a void fraction matching condition is imposed as the transition criteria. This model predicts that the transition occurs at the line of constant void fraction when both the gas and liquid phases are turbulent. A transition value of $\varepsilon = 0.8$ was determined for all flow maps using the 12.7 mm ID tube. The transition model for turbulent gas and laminar liquid is more complex, but the predicted

Table 1. Transition void fraction values for the bubble–slug transition

Fluids	Tube diameter (mm)	Transition void fraction
Air–water	12.7	0.40
Air–water/glycerin	12.7	0.36
Air–water/zonyl	12.7	0.46
Air–water	25.4	0.23
Air–water/glycerin	25.4	0.40
Air–water/zonyl	25.4	0.40

void fraction occurs at a nearly constant value of U_{GS}. This model over-predicted the transition void fraction in the turbulent liquid region, possibly due to problems in accurately determining the pressure gradient in the unstable slug–annular transition region.

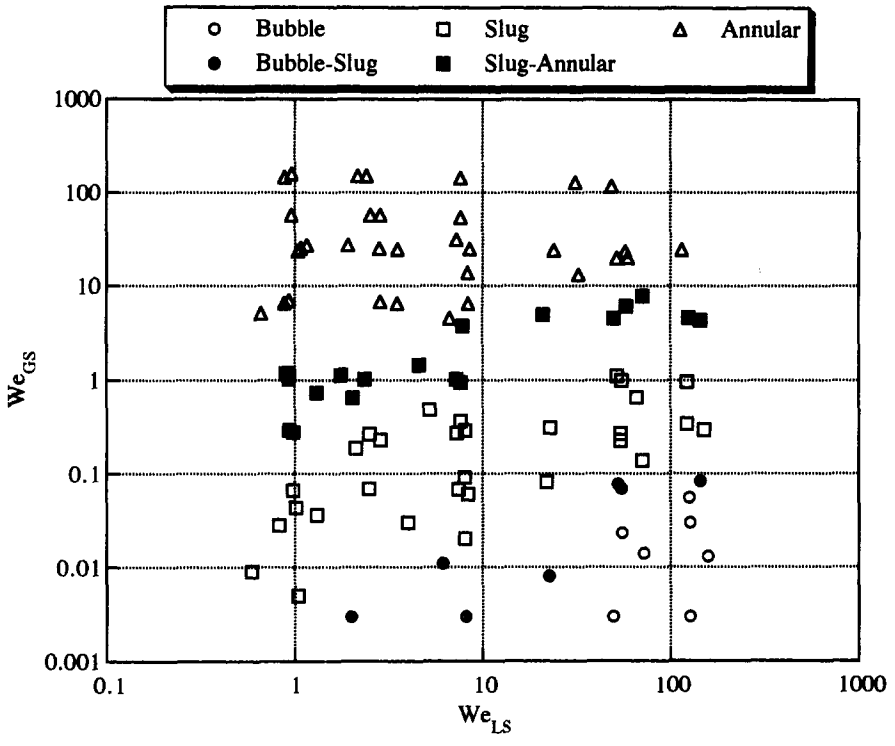

Figure 21. Microgravity Weber number flow pattern map for air–water in a 12.7 mm ID tube.

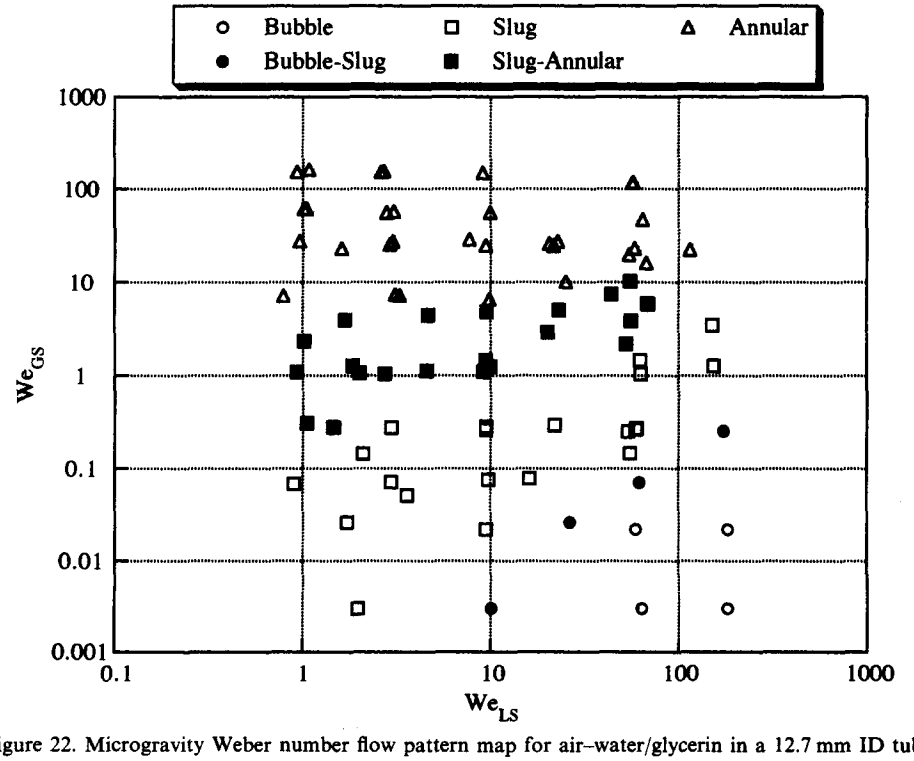

Figure 22. Microgravity Weber number flow pattern map for air–water/glycerin in a 12.7 mm ID tube.

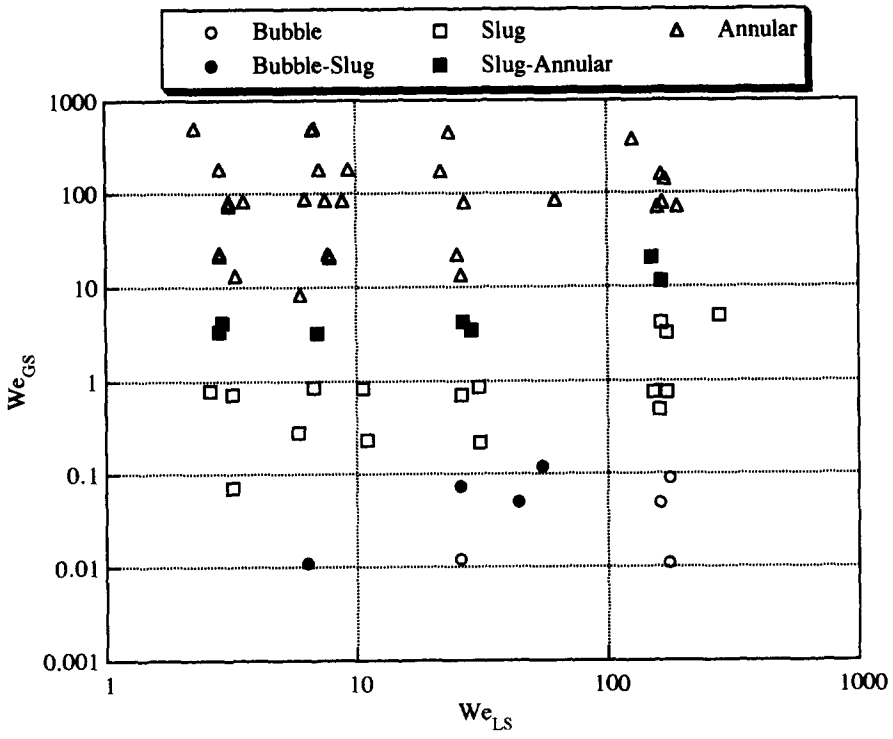

Figure 23. Microgravity Weber number flow pattern map for air–water/Zonyl FSP in a 12.7 mm ID tube.

The results of Bousman (1995) showed that the void fraction matching slug–annular transition model was very sensitive to the transition void fraction value used. If a line of constant void fraction at $\varepsilon = 0.75$ is used instead of that predicted from the more rigorous model, good separation of the slug and annular regimes is obtained for the air–water and air–water/Zonyl FSP flow pattern maps

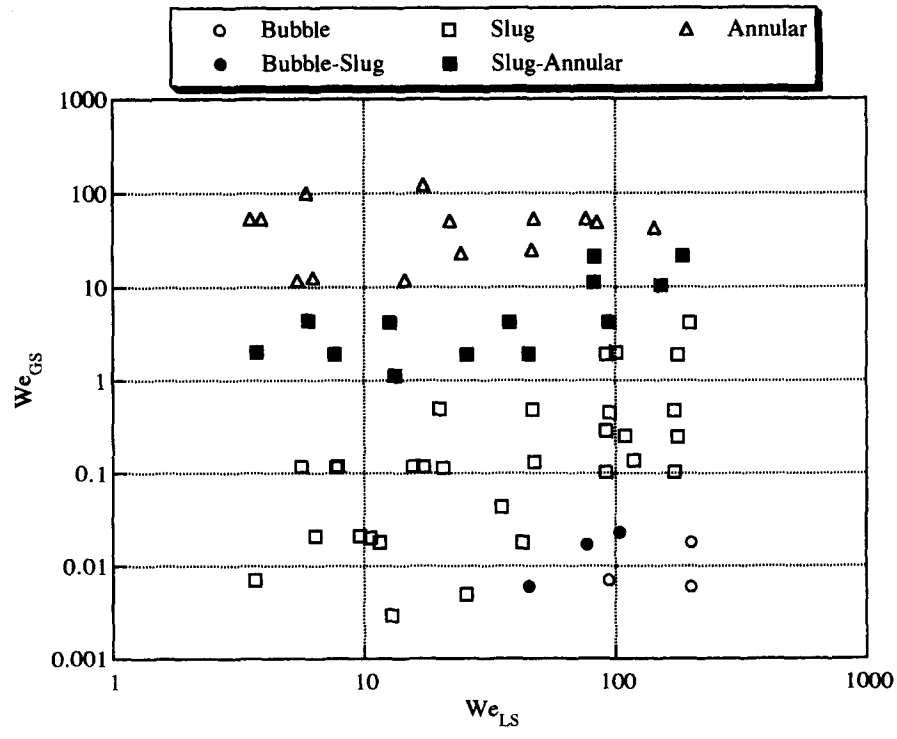

Figure 24. Microgravity Weber number flow pattern map for air–water in a 25.4 mm ID tube.

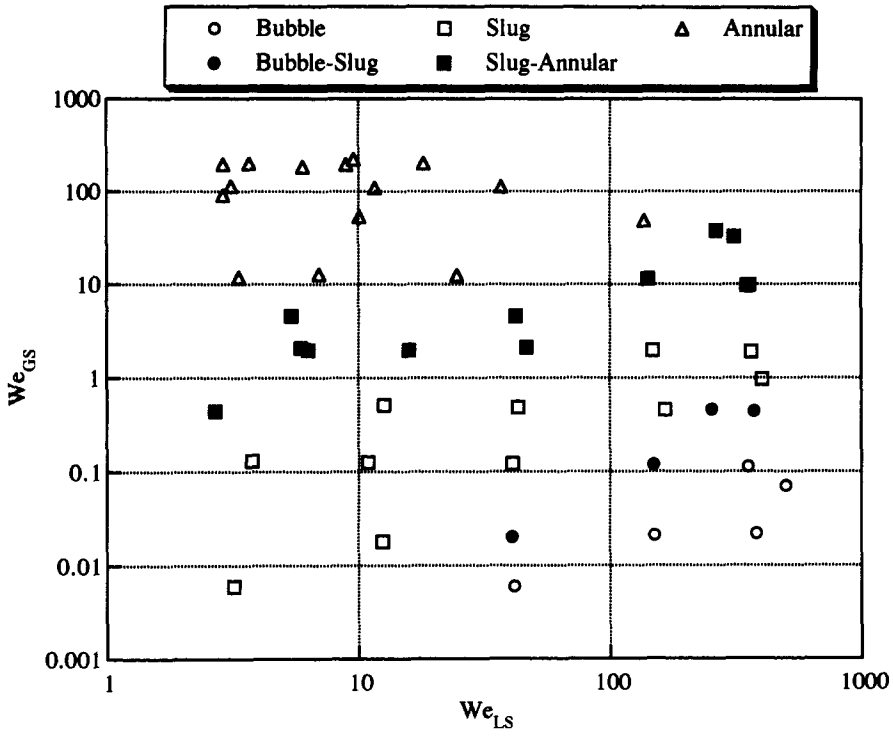

Figure 25. Microgravity Weber number flow pattern map for air–water/glycerin in a 25.4 mm ID tube.

for both tube diameters. A reasonable transition criterion for the air–water/glycerin flow pattern maps is $\varepsilon = 0.70$. These constant void fraction criteria are superimposed on the experimental flow pattern maps in figures 15–20.

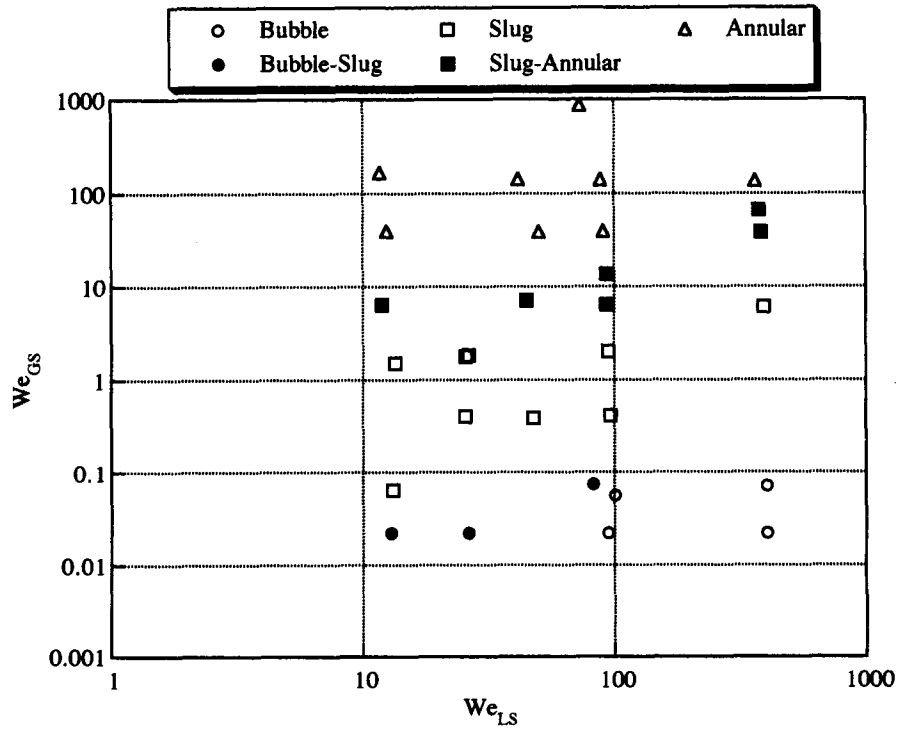

Figure 26. Microgravity Weber number flow pattern map for air–water/Zonyl FSP in a 25.4 mm ID tube.

WEBER NUMBER FLOW PATTERN TRANSITION MODELS

An alternative criteria for transition was proposed by Zhao & Rezkallah (1993) using the Weber number defined as

$$\mathrm{We} = \frac{\rho U^2 D}{\sigma}, \qquad [2]$$

where σ is the interfacial surface tension, U is the gas or liquid velocity, D is the tube diameter and ρ is the gas or liquid density. This represents the balance between inertial and surface tension forces. Flow pattern maps in terms of gas and liquid Weber numbers were presented in Zhao & Rezkallah (1993) and showed that the slug to slug–annular and slug–annular to annular transitions occurred at approximately $\mathrm{We_{GS}} = 1$ and $\mathrm{We_{GS}} = 20$, respectively. The authors propose that these values are the boundaries of surface tension and inertial force dominated regions of the flow pattern maps.

Flow pattern data collected in the present study were replotted in terms of gas and liquid Weber numbers as shown in figures 21–26. As shown, the boundaries of the slug–annular transition region appear to occur at approximately constant values of $\mathrm{We_{GS}}$ for $\mathrm{We_{LS}} < 100$ but not at higher values of $\mathrm{We_{LS}}$. This suggests that there may be merit to the concept of Weber number based transition models although another mechanism, responsible for the deviation at higher values of $\mathrm{We_{LS}}$, may also affect the flow pattern transitions.

7. SUMMARY

The ability to predict gas–liquid flow patterns is central to the design and operation of two-phase flow systems in the microgravity environment. Flow pattern maps have been developed which show the occurrence of flow patterns as a function of gas and liquid superficial velocities as well as tube diameter, liquid viscosity and surface tension. The results have demonstrated that the location of the bubble–slug transition is affected by tube diameter for air–water systems and by liquid viscosity and surface tension, suggesting that turbulence induced bubble fluctuations and coalescence mechanisms play a role in this transition. The location of the slug–annular transition on the flow pattern maps is largely unaffected by tube diameter, liquid viscosity or surface tension in the ranges tested. Void fraction based transition criteria were developed which separate the flow patterns on the flow pattern maps with reasonable accuracy. Weber number transition criteria also show promise but further work is required to improve these models.

Acknowledgements—This work is dedicated to the memory of Professor A. E. Dukler, University of Houston who passed away prior to the completion of this work. His wisdom and guidance laid the foundation for this study. The facilities and financial support provided by the NASA Lewis Research Center, Grant NAG3-510, the NASA Graduate Student Researcher's Program and the University of Houston, Department of Chemical Engineering are gratefully acknowledged.

REFERENCES

Baker, O. 1954 Simultaneous flow of oil and gas. *Oil and Gas J.* **53,** 185–195.

Barnea, D. 1986 Transition from annular flow and from dispersed bubble flow—unified models for the whole pipe range of inclinations. *Int. J. Multiphase Flow* **12,** 733–744.

Bousman, W. S. 1995 Studies of two-phase gas–liquid flow in microgravity. NASA Contractor Report 195434, NASA Lewis Research Center; also Ph.D. dissertation, University of Houston, U.S.A. 1994.

Brown, R. C., Andreussi, P. & Zanelli, S. 1978 The use of wire probes for the measurement of liquid film thickness in annular gas–liquid flows. *Can. J. Chem. Eng.* **56,** 754–757.

Colin, C. 1990 Ecoulements diphasiques a bulles et a poches en micropesanteur. M.Sc. thesis, Institut de Mecaniques des Fluides de Toulouse, France.

Colin, C., Fabre, J. & Dukler, A. E. 1991 Gas liquid flow at microgravity conditions—I. *Int. J. Multiphase Flow* **17,** 533–544.

Dukler, A. E., Fabre, J. A., McQuillen, J. B. & Vernon, R. 1988 Gas liquid flow at microgravity conditions: flow patterns and their transitions. *Int. J. Multiphase Flow* **14,** 389–400.

Huckerby, C. S. & Rezkallah, K. S. 1992 Flow pattern observations in two-phase gas–liquid flow in a straight tube under normal and microgravity conditions. *Proc. 1992 AIChE Heat Transfer Conference*, San Diego **88,** 139–147.

Janicot, A. J. P. 1988 Experimental and theoretical studies of gas–liquid two phase flow at reduced gravity conditions. M.Sc. thesis, University of Houston, U.S.A.

Lacy, C. E. 1992 Flooding and wavy films in vertical annular gas–liquid flows. Ph.D. dissertation, University of Houston, U.S.A.

Lekan, J. 1989 Microgravity research in NASA ground based facilities. NASA Technical Memorandum 101397.

McQuillen, J. B. & Neumann, E. S. 1995 Two-phase flow research using the Learjet apparatus. NASA Technical Memorandum 106814, NASA Lewis Research Center.

Reinarts, T. R. 1993 Adiabatic two phase flow regime data and modeling for zero and reduced (horizontal flow) acceleration fields. Ph.D. dissertation, Texas A&M University, U.S.A.

Swanson, T. D., Juhasz, A., Long, W. R. & Ottenstein, L. 1989 Proceedings of workshop on two-phase fluid behavior in a space environment. NASA Conference Publication 3043, NASA Headquarters.

Taitel, Y. & Dukler, A. E. 1976 A model for predicting flow regime transitions in horizontal and near horizontal gas–liquid flow. *AIChE J.* **22,** 47–55.

Zhao, L. & Rezkallah, K. S. 1993 Gas–liquid flow patterns at microgravity conditions. *Int. J. Multiphase Flow* **19,** 751–763.

Zuber, N. & Findlay, J. A. 1965 Average volumetric concentration in two phase flow systems. *J. Heat Transfer* 453–468.